A numerical investigation of flame liftoff, stabilization, and blowout

Alejandro M. Briones and Suresh K. Aggarwal[a)]
Department of Mechanical and Industrial Engineering, University of Illinois at Chicago, Chicago, Illinois 60607

Viswanath R. Katta
Innovative Scientific Solutions, Inc., 2766 Indian Ripple Road, Dayton, Ohio 45440

(Received 13 September 2005; accepted 28 February 2006; published online 17 April 2006)

The effects of fuel stream dilution on the liftoff, stabilization, and blowout characteristics of laminar nonpremixed flames (NPFs) and partially premixed flames (PPFs) are investigated. Lifted methane-air flames were established in axisymmetric coflowing jets. Because of their flame suppression characteristics, two predominantly inert agents, CO_2 and N_2, were used as diluents. A time-accurate, implicit algorithm that uses a detailed description of the chemistry and includes radiation effects is used for the simulations. The predictions are validated using measurements of the reaction zone topologies and liftoff heights of both NPF and PPF. While an undiluted PPF is stabilized at the burner rim, characterized by significant radical destruction and heat loss to the burner, the corresponding undiluted NPF is lifted and stabilized in a low-velocity region extending from the wake of the burner. Detailed comparison of diluted NPF with PPF reveals that the base structures of both the flames are similar and exhibit a double flame structure in the near-field region, where the flame stabilization depends on a balance between the reaction rate and the scalar dissipation rate, which could also be interpreted as a balance between the edge-flame speed undergoing its local scalar dissipation rate and the local flow velocity. As diluent concentration is increased, the flames become weaker, move downstream along the stoichiometric mixture fraction line, and stabilize at a location where they can find a local flow field that has a lower scalar dissipation rate. Further increase of the diluent concentration moves the flames further downstream into the far-field region, where both the NPF and PPF exhibit a triple flame structure, and the flame stabilization mechanism also involves a balance between the triple flame speed and local flow velocity. The PPFs, however, shift to a higher liftoff height and blow out at a lower diluent concentration compared to the NPF, which can withstand larger amounts of dilution. In addition, both NPF and PPF are stabilized at lower liftoff heights and blowout at a lower diluent concentration, when they are diluted with N_2 compared to that with CO_2. The observed effects of fuel stream dilution and partial premixing on flame liftoff and blowout can be explained using the existing flame stabilization theories. © *2006 American Institute of Physics*.
[DOI: 10.1063/1.2191851]

INTRODUCTION

Flame liftoff and blowout are important for both fundamental and practical considerations. In a coflow jet configuration, depending on fuel jet and coflow conditions (i.e., velocity, dilution, and amount of premixing), flames can be stabilized either at the burner or they can be lifted and stabilized downstream of the burner. Moreover, as liftoff height increases, the flame structure can transition from a nonpremixed flame to a double flame containing two reaction zones, and then to a triple flame containing three reaction zones, i.e., a lean premixed zone, a rich premixed zone, and a nonpremixed zone.[1] Phillips[2] first described these lifted triple flames. Subsequently, several stabilization criteria for lifted jet diffusion flames have been proposed.[3–8]

Most previous studies have based the flame stabilization mechanism in terms of a balance between the local flow velocity and the tribrachial flame speed. Chung and Lee[3] employed a cold jet theory,[9] and derived a theoretical formula for liftoff height and blowout conditions of nonpremixed jet flames. Their analysis showed that the Schmidt number (Sc) plays an important role in flame liftoff, and stable lifted flames are possible only for fuels for which $Sc > 1$. Increasing the fuel flow rate increases the liftoff height for propane and n-butane flames ($Sc > 1$) and decreases it for methane and ethane flames ($0.5 < Sc < 1$), implying that methane and ethane flames blowout directly in the burner-stabilized mode. However, Kioni *et al.*[10] and Plessing *et al.*[11] established lifted methane flames using nitrogen dilution and investigated the effect of strain rate. Ghosal and Vervisch[12] demonstrated analytically that a lifted laminar flame is possible for a fuel for which Sc is greater than a critical value Sc_{cr}, which is less than unity. For values of $Sc < Sc_{cr}$, they showed that a lifted flame is subcritical and can only survive in a narrow parametric region. In a subsequent study, Lee *et al.*[13] investigated the effect of partial premixing on flame liftoff and blowout for propane and

[a)]Author to whom all correspondence should be addressed. Electronic address: ska@uic.edu

n-butane flames, and observed that the jet velocity at flame liftoff and blowout decreases as the level of partial premixing is increased.

Ruetsch *et al.*[5] reported that the effect of heat release on lifted triple flames provides an upper bound for the flame speed. Increasing the heat release and reducing the mixture fraction gradient increases the flame speed over that of the corresponding planar premixed flame. Buckmaster[14] demonstrated that in a special case of unity Lewis number (Le), the edge flame speed (U_F) increases with decreasing scalar dissipation rate (χ) in a linear form, $U_F/S_L^o=1-\chi/\chi^o$, where χ_o is the scalar dissipation rate when U_F is zero. Chen and Bilger[6] reported that the flame propagation speed (U_P) increases monotonically with decreasing χ along the stoichiometric mixture fraction contour. They combined the above theories to propose a general expression for the triple flame propagation velocity, $U_P/S_L^o=(\rho_u/\rho_b)1/2[1-(\chi_{st}/\chi_a)^m]$, where the correlation constants m and χ_a are determined from a linear regression analysis. This equation is consistent with the argument that U_P/S_L^o is bounded by the heat release for small scalar dissipation rates. Based on the above flame stabilization theories, most previous investigations have focused on determining the critical inlet flow velocities for flame liftoff and blowout. However, the liftoff and blowout characteristics of NPFs, and especially those of PPFs, with respect to the effects of diluents, have not been extensively investigated. This provided the major motivation for the present study.

The flame stabilization theories[3–6] described above are based on the tribrachial flame speed hypothesis. Takahashi and Katta[8] reported, however, that flames stabilized near the burner do not exhibit a triple flame structure, and therefore the flame stabilization cannot be explained in terms of the tribrachial flame speed. Instead they hypothesized that a lifted nonpremixed flame is stabilized by a reaction kernel, in which a subtle balance is maintained between the residence time and reaction time. They also highlighted the importance of detailed chemistry in simulating flame liftoff and stabilization, as global chemistry, which neglects the radical reactions, led to an incorrect understanding of the flame base or reaction kernel structure.

Studies dealing with the effects of diluents on the liftoff and blowout characteristics of flames are also important for practical considerations. For instance, Halon 1301 is currently used worldwide for fire protection, but because of concerns with its effect on the stratospheric ozone layer, it is regulated by international agreements (Montreal Protocol[15]). While these regulations have intensified research for new fire suppressants, the search for a new fire-extinguishing agent with all the desirable properties of Halon 1301 has not been successful so far. Vahdat *et al.*[16] investigated flame extinction using binary fire suppressants of organic compounds mixed with nitrogen. Although these mixtures appear to be promising, halogenated compounds such as CF_3Br (Halon 1301) are still found to be more efficient. The inert gases extinguish fire primarily through the thermal effect, and thus being harmless to the environment, provide justification for studying their effects on lifted flames.

The major objective of our investigation is to characterize the effects of fuel stream dilution and partial premixing on flame liftoff, stabilization, and blowout. Lifted methane-air nonpremixed (NPF) and partially premixed flames (PPFs) are established in axisymmetric coflowing jets. The flames are simulated using a time-accurate, implicit algorithm that uses detailed descriptions of chemistry and transport. Results of simulations are used to (i) distinguish between the burner-stabilized and lifted flames in terms of velocity profiles along the stoichiometric mixture fraction line and heat transfer from the flame to the burner, (ii) perform a detailed comparison of the structures of NPF and PPF in terms of the various reaction zones near the flame base; the base flame structure is important for the flame stabilization criteria, (iii) examine the flame stabilization criteria for lifted flames stabilized in both the near-field and far-field regions, and (iv) characterize the effectiveness of two common fire suppression agents, N_2 and CO_2, in extinguishing the NPFs and PPFs.

Depending on the liftoff height, diluent concentration, and other conditions, the liftoff behavior of nonpremixed jet flames falls into three different categories:[17] (i) both liftoff and blowout occurring in the laminar region, (ii) liftoff occurring in the laminar region, but blowout in the turbulent region, and (iii) both liftoff and blowout occurring in the turbulent region. In the present study, we focus on the liftoff and blowout occurring in the laminar region of coflowing jets. A coflow jet configuration is employed, since it provides more stable flow conditions compared to free jets, and also facilitates the treatment of boundary conditions.

THE COMPUTATIONAL MODEL

The computational model is based on the algorithm developed by Katta *et al.*[18] and the simulation method is described in detail elsewhere.[19,20] The numerical model solves the time-dependent governing equations for unsteady reacting flows in an axisymmetric configuration. The governing equations can be written in a generalized form as

$$\frac{\partial(\rho\Phi)}{\partial t}+\frac{\partial(\rho v\Phi)}{\partial r}+\frac{\partial(\rho u\Phi)}{\partial z}=\frac{\partial}{\partial r}\left(\Gamma^{\Phi}\frac{\partial\Phi}{\partial r}\right)+\frac{\partial}{\partial z}\left(\Gamma^{\Phi}\frac{\partial\Phi}{\partial z}\right)-\frac{\rho v\Phi}{r}+\frac{\Gamma^{\Phi}}{r}\frac{\partial\Phi}{\partial r}+S^{\Phi}.$$

Here t denotes the time, and u and v represent the axial (z) and radial (r) velocity components, respectively. The general form of the equation represents conservation of mass, momentum, species, or energy conservation equation, depending on the variable used for Φ. The diffusive transport coefficient Γ^{Φ} and source terms S^{Φ} appearing in the above equation are provided in Table 1 of Ref. 19. Introducing the overall species conservation equation and the state equation completes the set of equations. In addition, a sink term based on an optically thin gas assumption is included in the energy equation to account for thermal radiation from the flame.[25] The sink term is expressed as $q_{rad}=-4\sigma K_p(T^4-T_o^4)$,[21] where T denotes the local flame temperature, and K_p accounts for the absorption and emission from the participating gaseous

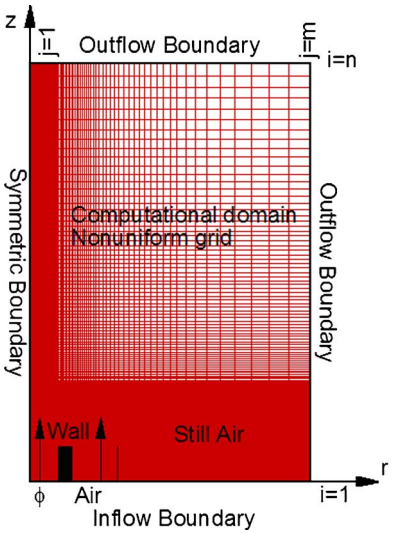

FIG. 1. Schematic of the computational domain and boundary conditions.

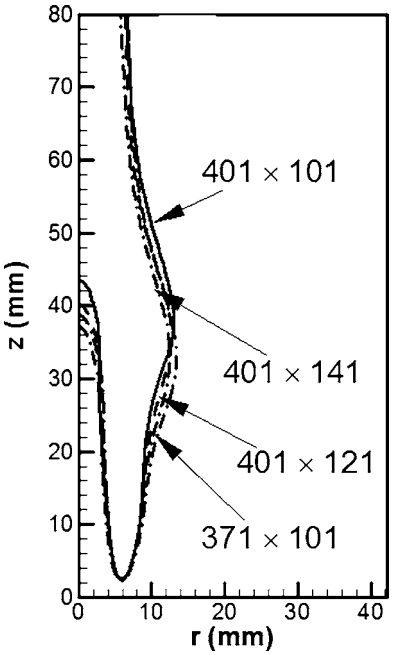

FIG. 2. Temperature isocontour of 1000 K for a CO_2-diluted partially premixed flame computed using four different grids. For all cases, the flame is computed using the same initial conditions.

species (CO_2, H_2O, CO and CH_4), and is expressed as $K_p = P\sum_k X_i K_{p,i}$, where $K_{p,i}$ denotes the mean absorption coefficient of the kth species. Its value is obtained by using a polynomial approximation to the experimental data provided in Ref. 21.

The thermodynamic and transport properties appearing in the governing equations are considered to be temperature- and species-dependent. The thermal conductivity and viscosity of the individual species are estimated based on Chapman–Enskog collision theory, following which those of the mixture are determined using the Wilke semiempirical formulas.[22] Chapman–Enskog theory and the Lennard–Jones potentials are used to estimate the binary-diffusion coefficient between each species and nitrogen. The methane–air chemistry is modeled using a detailed mechanism that considers 24 species and 81 elementary reactions.[23] The major species included in the mechanism are CH_4, O_2, CO_2, CO, CH_2O, H_2, H_2O, C_2H_2, C_2H_4, C_2H_6, and N_2, while the radical species include CH_3, CH_2, CH, CHO, H, O, OH, HO_2, H_2O_2, C_2H, C_2H_3, C_2H_5, and CHCO. The mechanism has been validated previously for the computation of premixed flame speeds and the detailed structure of both nonpremixed and partially premixed flames.[19,20,24–26]

While the finite-difference forms of the momentum equations are obtained using the QUICKEST scheme,[27] those of the species and energy are obtained using a hybrid scheme of upwind and central differencing. The pressure field is calculated at every time step by solving all of the pressure Poisson equations simultaneously and using the LU (lower and upper diagonal) matrix-decomposition technique.

Figure 1 illustrates the computational domain. It consists of 150 mm × 100 mm in the axial (z) and radial (r) directions, respectively, and is represented by a staggered, nonuniform grid system. The reported results are grid-independent, as discussed in the next section. An isothermal insert simulates the inner 2 × 1 mm burner wall. The boundary conditions used here can be found elsewhere.[19,20] Both the inner and outer jets are set with a constant and uniform velocity of 50 cm/s. The inner jet issues fuel-air mixture at equivalence ratios of $\phi=\infty$ (pure fuel) and 2.25 for the simulation of nonpremixed and partially premixed flames, respectively, while the outer jet issues air. The diluent (CO_2 or N_2) is introduced through the inner jet, and its concentration is varied in order to investigate the flame liftoff, stabilization, and blowout phenomena.

The two base cases simulated correspond to undiluted NPF and PPF. These two base flames are obtained starting from the respective global-chemistry ($CH_4+O_2 \rightarrow CO_2+H_2O$) solutions as initial conditions and by performing detailed-chemistry calculations for sufficiently long times (~10000 time steps corresponding to 2 s).[23] Once the undiluted flames are established, diluents are gradually added until blowout is reached. Blowout is achieved when a critical concentration of diluents moves the flames further downstream rapidly and out of the computational domain, as described by Katta *et al.*[28]

RESULTS AND DISCUSSION

Validation of numerical model

Egolfopoulos and Law[29] demonstrated that by minimizing the effect of numerical diffusivity through mesh refinement, the computed flame speed, which plays a key role in flame stabilization, converges to a grid-independent value. Results of numerical simulations to achieve grid independence for the present case are illustrated in Fig. 2, which presents an isotemperature contour (1000 K) for a typical CO_2–diluted PPF computed using four different grids, i.e., 371 × 101, 401 × 101, 401 × 121, and 401 × 141. The mole fraction of CO_2 added to the fuel stream is 5% for this case. For all four grids, the calculations begin using the same ini-

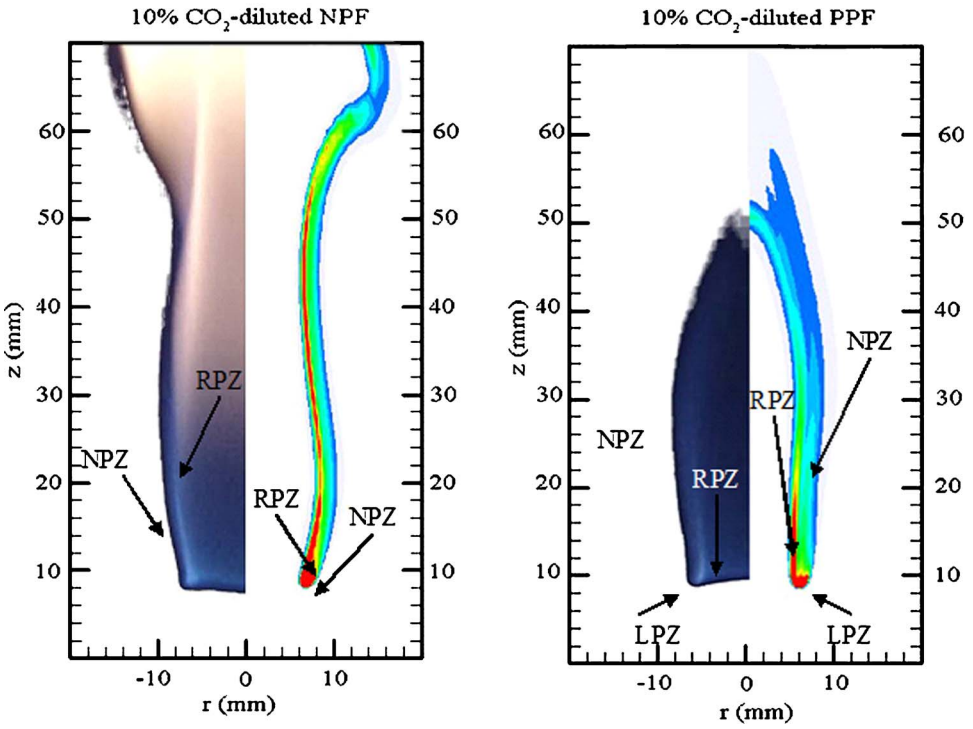

FIG. 3. Comparison of predicted heat release rate contours (right) and measured luminosity contours (left) for the 10% CO_2-diluted nonpremixed (NPF) and partially premixed flames (PPF). The rich premixed, nonpremixed, and lean premixed reactions zones are represented by RPZ, NPZ, and LPZ, respectively.

tial conditions. Grid lines are clustered near the flame surfaces (not shown) to resolve the steep gradients of the dependent variables. The differences between the results computed using these four grids are small, suggesting the convergence of the simulated flame. Therefore, the minimum grid spacing used for our simulations is 0.103 mm in the z direction and 0.150 mm in the r direction corresponding to a 401×101 grid. In order to further assure that both the temperature and radical species layers are sufficiently resolved in our simulations, we plotted (not shown) the radial profiles of temperature and CH radical near the lifted flame base (at an axial distance of 10.0 mm from the flame base). The thicknesses of the temperature and CH radical layers computed from these profiles were found to be 7.9 and 1.2 mm, respectively. We also computed the structure of the corresponding PPF established at $\phi=2.25$ in a counterflow (one-dimensional) configuration, and found (not shown) that the temperature and CH radical layers had thicknesses of 7.7 and 1.5 mm, and contained 47 and 10 grid points, respectively. These results provided additional confirmation that both the temperature and radical layers are sufficiently resolved in our simulations.

The numerical model has been previously validated using experimental data for a variety of steady and unsteady flames, including opposed-jet diffusion flames,[30] burner-stabilized flames,[20,31,32] and lifted flames.[7,28] Katta *et al.*[30] compared the predicted OH concentrations in opposed-jet flames with the measurements from planar laser-induced fluorescence (PLIF), and showed good agreement. Shu *et al.*[31] reported good agreement between the predicted and the measured velocity fields using PIV, as well as between the predicted heat release rate contours and the measured C_2^*-chemiluminescence images, for methane-air partially premixed flames. Azzoni *et al.*[20] reported similarly good agreement for triple flames stabilized on a slot burner. Likewise, Takahashi *et al.*[7] reported good agreement between the predicted and measured velocity fields using particle imaging velocimetry (PIV) for methane-air jet diffusion flames under near-lifting conditions. Recently, Katta *et al.*[28] accurately predicted the minimum diluent concentration for blowout of methane-air cup-burner flames.

In the present study, we provide additional validation of the numerical model by comparing the predicted heat release rate contours with the measured luminosity contours for CO_2-diluted lifted nonpremixed and partially premixed flames. As shown in Fig. 3, the numerical model reproduces the measured flame topology and liftoff height for both NPF and PPF. Both flames are located about 9 mm above the burner rim. Mixing of the reactants is enhanced in the wake region above the burner rim, allowing entrainment of air into the fuel side. Consequently, the NPF exhibits a double flame structure containing a rich premixed zone and a nonpremixed zone, while the PPF exhibits a triple flame structure. The locations of the various reaction zones are well predicted by the numerical model. The detailed flame structure for these cases is discussed in a later section. As these flames are established at normal gravity, both the simulations and measurements exhibit well-organized oscillations, induced by buoyant acceleration, and so care is taken in comparing the two flames at the same phase angle. In the NPF, the buoyant acceleration of hot gases outside the flame surface causes shear-layer rollup, leading to the formation of a toroidal vortex that interacts with the flame surface at locations downstream of the flame base. On the other hand, the PPF does not indicate this toroidal vortex ring; instead, the flame pinches off when the flame tip reaches its maximum amplitude. The blue color in the experimental images represents the flame shape and the bright yellow in the NPF corre-

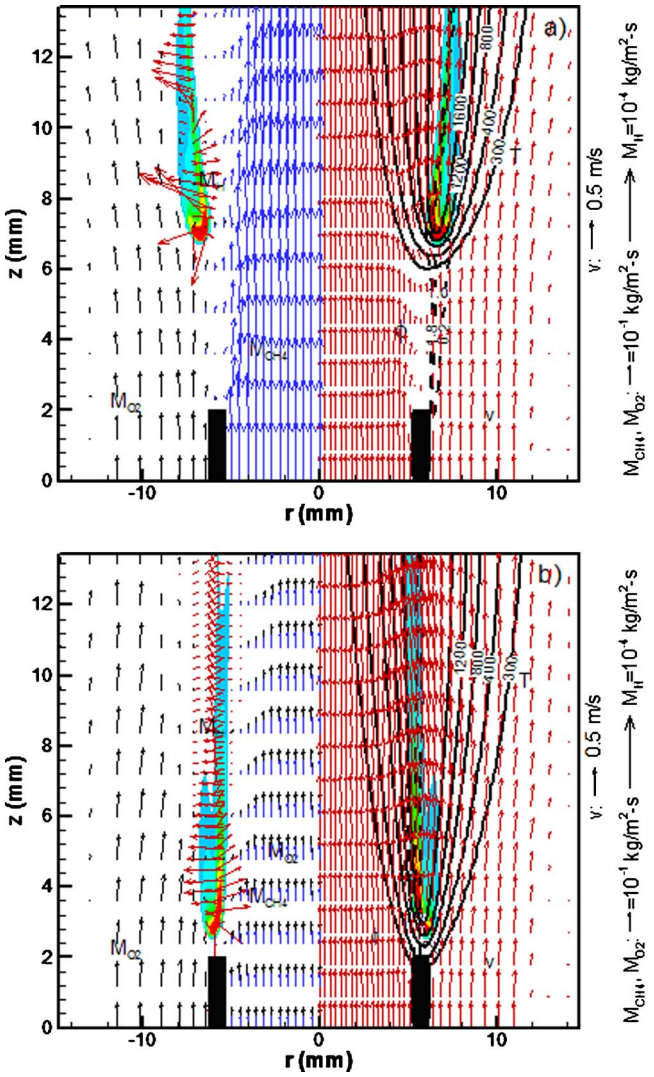

FIG. 4. Computed temperature contours (T), equivalence ratio contours (ϕ), heat release rate contours (q), velocity vectors (v), and mass flux vectors of $CH_4(M_{CH4})$, $O_2(M_{O2})$, and H-atoms (M_H) for the undiluted (a) NPF and (b) PPF. The mass flux vectors are shown on the left side, while q-contours are shown on both sides of the axis of symmetry.

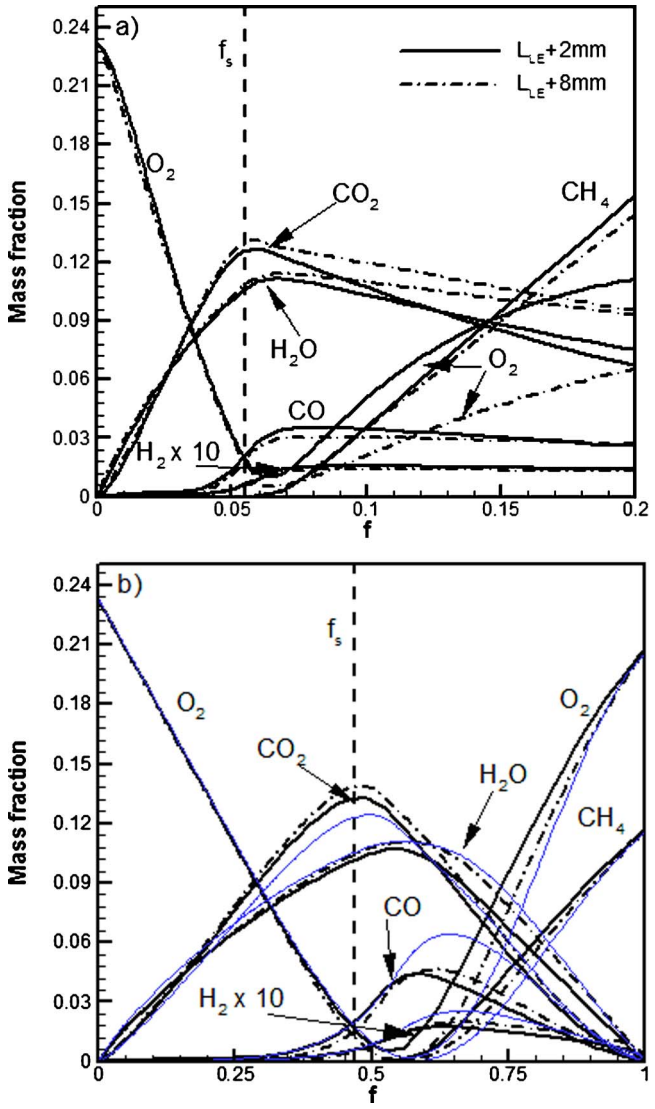

FIG. 5. State relationships in terms of scalar profiles at two axial locations with respect to mixture fraction (f) for the (a) NPF and (b) PPF discussed in the context of Fig. 4. An analogous steady counterflow flame at $\phi=2.25$ and strain rate of 100 s^{-1} is also shown for comparison with the coflow PPF in Fig 5(b). The thin blue lines represent the results from the counterflow flame. The vertical dashed line represents the stoichiometric mixture fraction (f_s).

sponds to the soot-containing region. Notice that the flame luminosity is greatly diminished in the PPF, implying a significant reduction in soot volume fraction due to partial premixing. Although the numerical model does not account for soot formation, which enhances thermal radiation, the liftoff heights between the experiments and simulations match quite well. This is mainly due to a lack of soot in the flame-base region and, hence, ignoring soot and the related thermal radiation in the numerical simulations did not affect the accuracy of the predicted flame base structure.

Structure of undiluted nonpremixed and partially premixed flames

Figure 4 presents the computed flame structures of the undiluted NPF and PPF in terms of temperature contours (T) (in solid lines), equivalence ratio contours (ϕ) (in broken lines), and velocity vectors (v) on the right side and mass flux vectors (M_{CH4}, M_{O2}, and M_H) on the left side of the axis of symmetry. The heat release rate contours (q) (in rainbow color scheme) are shown on both sides. As noted earlier, these flames at normal gravity exhibit well-organized oscillations. Consequently, the plots in Fig. 4 depict the instantaneous flame structure. For the NPF, the flame base is lifted and stabilized in a low-velocity region that extends from the wake of the burner rim. The mixing of the reactants is enhanced in the wake region, as indicated by the overlapping of CH_4 and O_2 mass flux vectors and the equivalence ratio contours. The flame is located on the air side, where the flame reaches stoichiometric conditions. The heat release rate contours show the high reactivity region near the flame base. The velocity vectors show the thermal expansion, as well as the axial acceleration, as the flow approaches the hot flame. Because the flame base was formed on the air side (due to the low value of stoichiometric ratio for methane fuel and

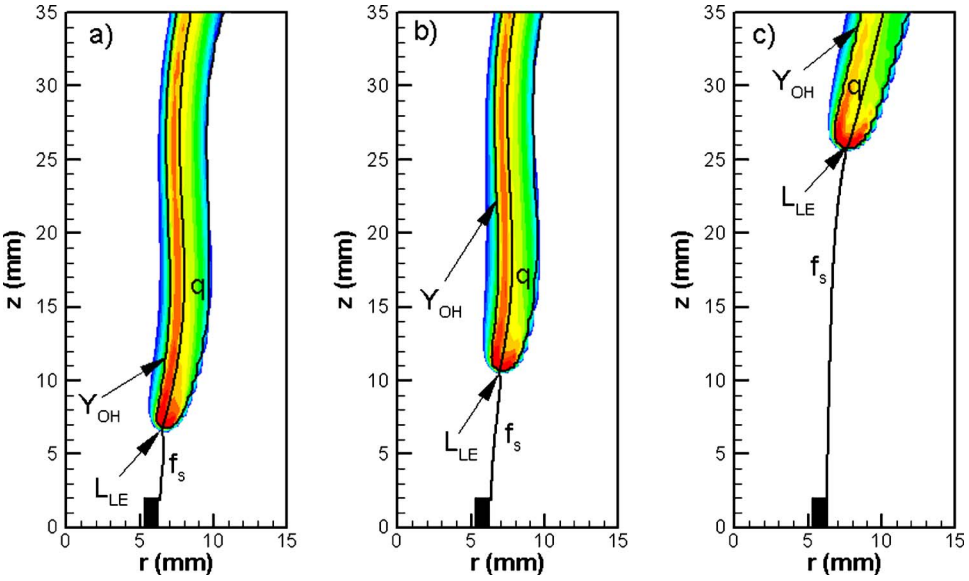

FIG. 6. Predicted heat release rate contours (q), stoichiometric mixture fraction line (f_s), and OH mass fraction (Y_{OH}) contours for three cases: (a) undiluted, (b) 15% CO_2-diluted, and (c) 30% CO_2-diluted NPFs. The location of the leading edge is indicated by L_{LE}.

oxygen), the mass flux of O_2 dominates compared to that of CH_4. Consequently, the high oxygen concentration that surrounds the flame base and the H atoms that diffuse in every direction enhance the chain-branching reaction $H+O_2 \rightarrow OH+O$, as discussed by Takahashi and Katta.[8]

In summary, the NPF is lifted and stabilized downstream of the burner on the oxidizer side with negligible heat transfer to the burner, while the PPF is stabilized at the burner rim with a significant heat transfer to the burner, as indicated by the temperature contours near the burner rim in Fig. 4(b). This implies that partial premixing affects flame stabilization near the burner rim. This can be expected since the flame stabilization near the burner has been argued to depend upon the leakage of oxygen to the fuel side.[33,34] Since oxygen is already present in the fuel stream for the PPF, its stabilization behavior is expected to be different from that of the corresponding NPF. These two flames also provide a clear distinction between the characteristics of the lifted and burner-stabilized flames.

In order to further examine the structures of the two flames depicted in Fig. 4, we present in Fig. 5 the state relationships in terms of the profiles of major reactant and product species (CH_4, O_2, H_2O, and CO_2), and "intermediate" fuel species (H_2 and CO) with respect to the mixture fraction (f).[35] Here f=1 and 0 indicate the fuel and oxidizer sides, respectively. Scalar profiles for a counterflow flame simulation at $\phi=2.25$ and strain rate 100 s^{-1} are also included for comparison with the coflow PPF. As discussed by Smooke[36] and Naha and Aggarwal,[37] partially premixed combustion can be grouped into two distinct regimes, namely a double-flame regime and a merged-flame regime. In the first regime, a PPF contains two physically separated reaction zones, while in the second regime, the two reaction zones are nearly merged. In both the coflow and counterflow PPFs [cf. Fig. 5(b)], the incoming CH_4 and O_2 from the fuel side are completely consumed in the rich premixed zone before reaching the stoichiometric mixture fraction (f_s). The "intermediate" fuel species CO and H_2 are formed in the rich premixed zone, and then transported and consumed in the nonpremixed zone. The CO_2 and H_2O mass fractions, however, peak near the rich premixed zone, indicating a nearly merged-flame structure. The NPF also shows a similar flame structure in terms of the relative locations of the consumption of reactants and the peak intermediate species. The smaller f_s value for NPFs implies that more mixing is required for establishing these flames compared to that of PPFs. Also, note that the mass fraction of oxygen penetrating into the fuel side of NPF, $Y_{O2} \sim 0.12$, is comparable to the corresponding value, $Y_{O2} \sim 0.20$, for PPF. Since state relationships of both NPF and PPF are similar, these flames contain a nearly merged flame structure corresponding to a (double) partially premixed flame.

Effect of dilution on the lifted flame structure

Figure 6 presents the global flames structure of CO_2-diluted NPFs in terms of the heat release rate (q), stoichiometric mixture fraction (f_s), and OH mass fraction (Y_{OH}) contours for three different dilution levels. The flame leading edge (L_{LE}) is defined as the intersection of the stoichiometric mixture fraction (f_s) line and the flame surface, which is represented by a specific OH mass fraction contour (i.e., $Y_{OH}=2\times10^{-5}$), following Qin *et al.*[38] As expected, the liftoff height (L_f), which is taken as the distance from the burner rim to L_{LE}, increases, and L_{LE} shifts radially outward with increasing diluent concentration.

Previous investigations have generally distinguished the various reaction zones in jet flames based on their spatial locations.[19,39] In lifted flames, however, the premixing ahead of the flame front can be relatively small depending upon the liftoff height, and it may be difficult to distinguish between the double and triple flame structures at the flame base. This distinction, however, is important in the context of examining the flame stabilization mechanisms. In order to spatially resolve the various reaction zones of the flames more clearly, we employ the modified flame index (ξ_M) developed in our previous investigation,[1]

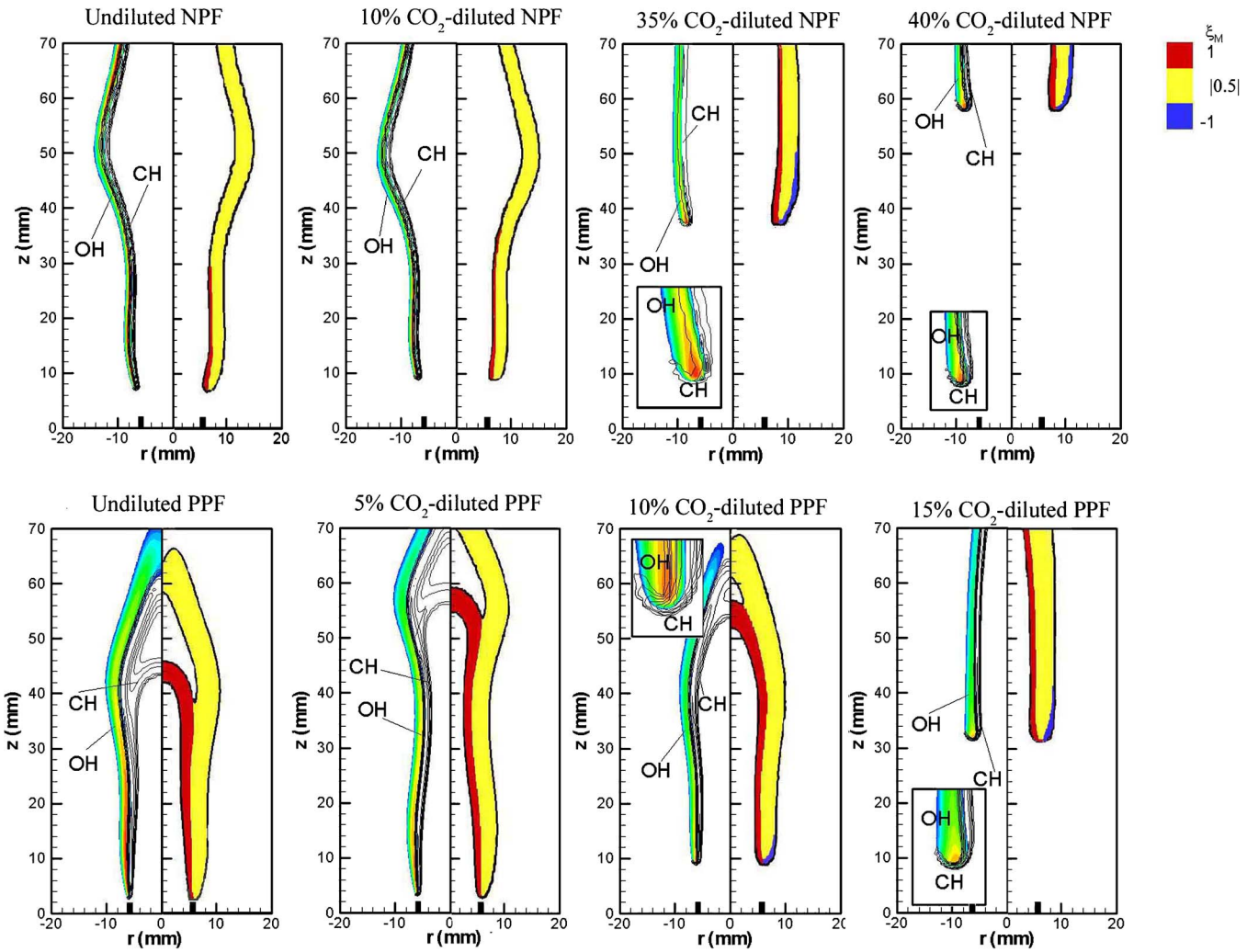

FIG. 7. Flame structures of various CO_2-diluted NPFs and PPFs are shown through the modified flame index (ξ_M) contours (right), the OH (color rainbow) and CH (monochrome) mass fraction contours (left). For NPFs, a double flame structure [with a rich premixed zone (RPZ) and a nonpremixed zone (NPZ)] is indicated for 0% and 10% CO_2-dilutions, and a triple flame structure for 35% and 40% CO_2-dilutions. For PPFs, a double flame structure is indicated for 0% and 5% CO_2-dilutions, and a triple flame structure for 10% and 15% CO_2-dilutions.

$$\xi_M = \left(\frac{f - f_s}{|f - f_s|}\right) \cdot \frac{1}{2}\left(1 + \frac{G_{\mathrm{FO}}}{|G_{\mathrm{FO}}|}\right).$$

Here the mixture fraction (f) is defined following Bilger,[35] and G_{FO} is the flame index proposed by Takeno and co-workers.[40] With this definition, $\xi_M = 1$ represents a rich premixed zone, -1 a lean premixed zone, and $|0.5|$ a nonpremixed zone for hydrocarbon flames. Since identification of the various reaction zones is more relevant in regions of high reactivity, i.e., where the heat release rates are significant, we have computed ξ_M only in regions where the heat release rate is at least 1% of the maximum heat release rate.

Figure 7 presents ξ_M contours as well as the OH (rainbow color) and CH (monochrome) mass fraction contours for NPFs and PPFs established at various CO_2-dilution concentrations. The CH and OH mass fractions have previously been used to indicate the flame structure in counterflow configuration.[36,41] Whereas the OH mass fraction peaks in the nonpremixed reaction zone when the flame exhibits a nearly merged flame structure, the CH mass fraction peaks in the premixed reaction zones, Therefore, OH and CH contours can also be used to visualize the flame structure, in addition to the modified flame index (ξ_M). As noted earlier, the undiluted NPF is lifted and stabilized at an axial location downstream of the burner rim wake. As the diluent concentration increases, L_f increases, and there is a transition from a double flame to a triple flame structure, characterized by the appearance of a lean premixed zone indicated by the blue color and the presence of CH in the outermost region of the flame base (i.e., the lean premixed zone). In contrast, for low diluent concentrations, the PPF is stabilized at the burner rim and exhibits a double flame structure. As the diluent concentration increases, the PPF is lifted. Further increase in diluent concentration increases L_f, and additional mixing in the region between burner rim and flame leads to a transition from a double flame to a triple flame structure. The lean premixed zone becomes more pronounced as L_f increases with the increase in diluent concentration. Therefore, the base structure of a lifted flame depends largely on L_f, which in turn de-

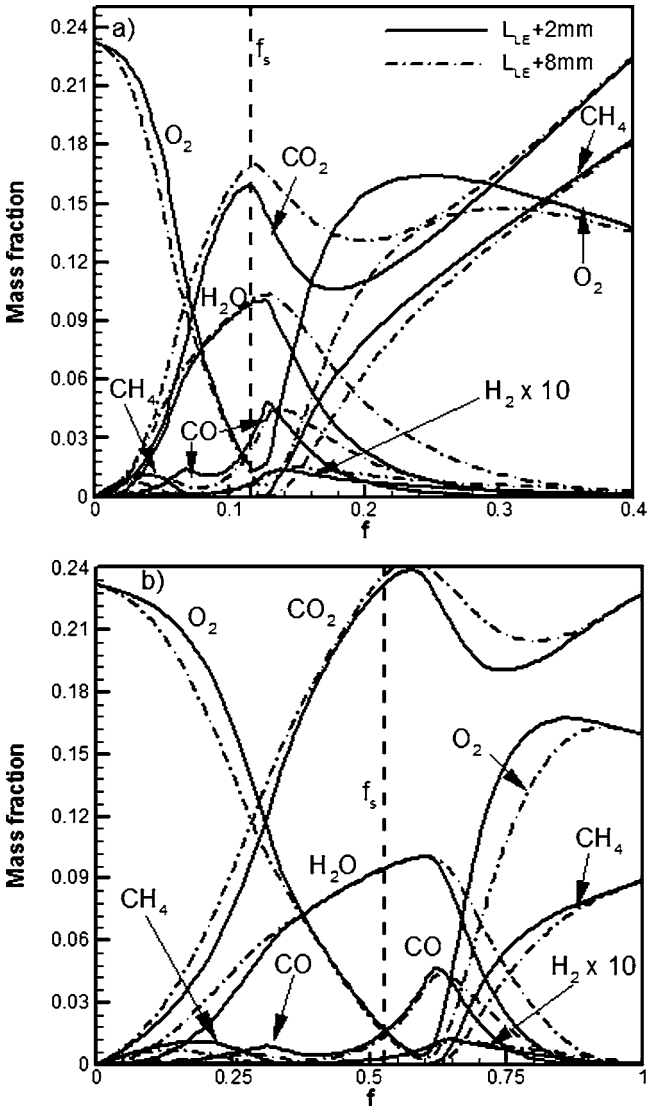

FIG. 8. State relationships in terms of scalar profiles with respect to mixture fraction (f) at two axial locations for (a) 20% CO_2-diluted NPF and (b) 10% CO_2-diluted PPF. The vertical dashed line represents the stoichiometric mixture fraction (f_s) value.

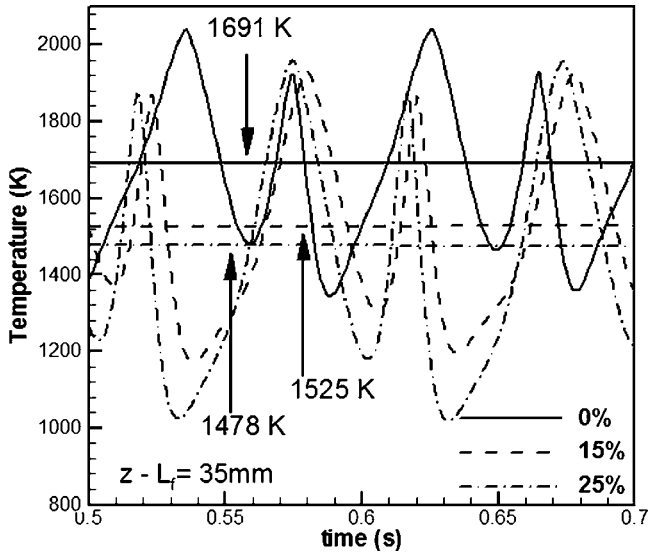

FIG. 9. Temporal evolution of temperature for undiluted, 15% CO_2-diluted, and 25% CO_2-diluted NPFs. The horizontal lines indicate the time-averaged temperature. The temperature values are taken 35 mm above the leading edge of each flame.

pends on mixture composition (i.e., diluent concentration, partial premixing, and premixing outside the nozzle[38,42]), jet velocity, coflow velocity, and nozzle shape.

Figure 8 presents the detailed structure of a 20% CO_2-diluted NPF and a 10% CO_2-diluted PPF. State relationships are presented for the major reactant and product species (CH_4, O_2, H_2O, and CO_2) and the "intermediate" fuel species (H_2 and CO) with respect to f[35] at two axial locations. The existence of a rich premixed zone in both the flames is indicated by the relatively high mass fraction of O_2 on the fuel side ($Y_{O2} \sim 0.16$). In this zone, both CH_4 and O_2 are completely consumed, producing "intermediate" fuel species H_2 and CO, which are transported and oxidized in the nonpremixed zone to form CO_2 and H_2O. The nonpremixed zone is located near $f=f_s$, as indicated by the peak mass fractions of CO_2 and H_2O. The leakage of CH_4 to the air side leads to the formation of a lean premixed reaction zone, which is located near $f=0.07$ and 0.3 for the NPF and PPF, respectively. The existence of a lean premixed zone is also illustrated by the comparison of flame structures depicted in Figs. 6 and 8. The location of the lean premixed zone is indicated by the second (smaller) CO and H_2O peaks in both NPF and PPF in Fig. 8. These peaks are located near $f=0.07$ and 0.3 for the NPF and PPF, respectively.

Buoyancy-induced flame oscillations

As noted earlier, the flames simulated in the present study exhibit well-organized oscillations induced by buoyant acceleration. In order to characterize these oscillations, Fig. 9 presents the temporal evolution of temperature at a location 35 mm above the flame leading edge for three CO_2-diluted NPFs. The interaction between the flame surface and the toroidal vortex, formed by buoyant acceleration of hot gases outside the flame surface, leads to oscillations in temperature. As the diluent concentration is increased and the flame is stabilized at a further downstream location, the amplitude of oscillation increases, while the frequency of oscillation remains nearly constant in the range 15–20 Hz. (The amplitude of oscillation refers to the amplitude of temperature variation at the probing point.) In addition, the mean temperature decreases, indicating a reduction in flame reactivity with increased dilution.

Effects of partial premixing and dilution on flame liftoff and blowout

In order to characterize the effects of partial premixing and diluents, the variation of flame liftoff height with diluent mole fraction is presented in two different formats. Figure 10 depicts the effect of partial premixing by plotting the liftoff height versus the amount of dilution in N_2-diluted flames [Fig. 10(a)] and CO_2-diluted flames [Fig. 10(b)], while Fig. 11 compares the effectiveness of N_2 and CO_2 diluents in

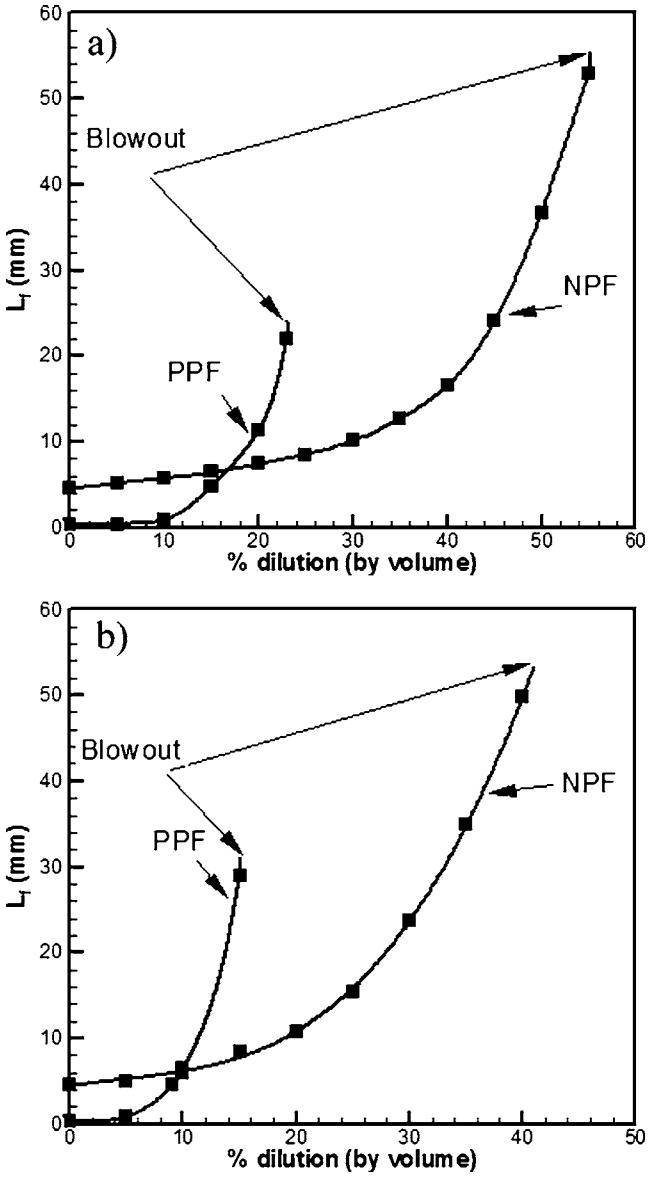

FIG. 10. Liftoff height (L_f) plotted as a function of diluent mole fraction for the N_2- (a) and CO_2-diluted (b) NPFs and PPFs. The blowout conditions are also shown.

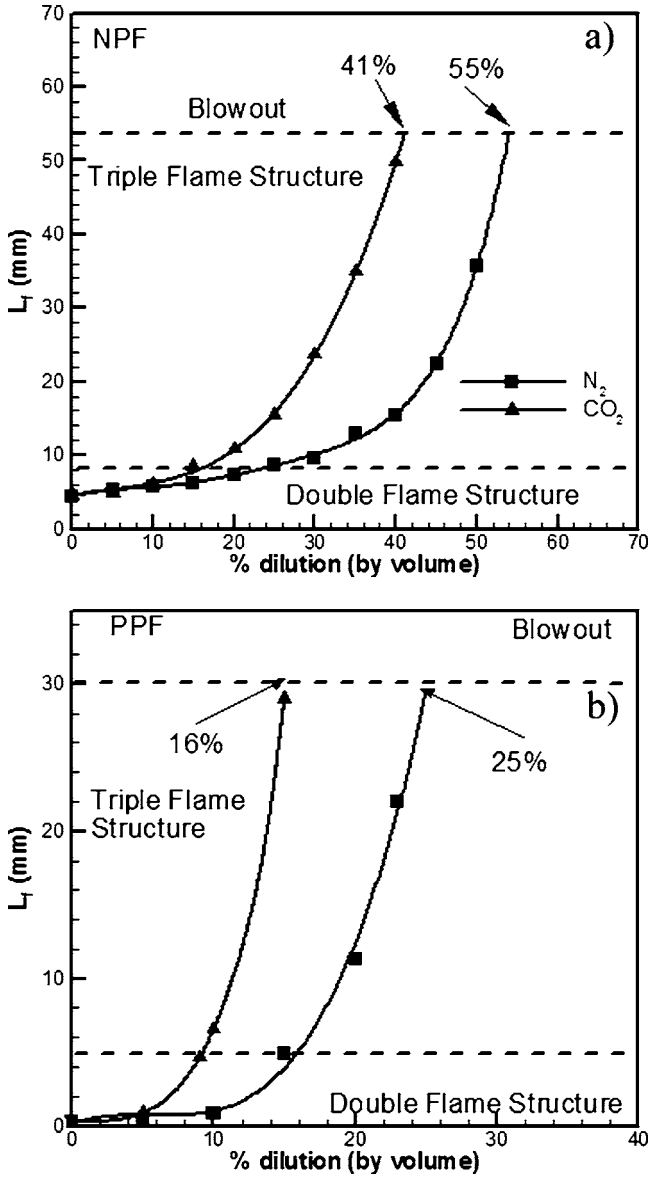

FIG. 11. Liftoff height (L_f) plotted as a function of diluent mole fraction for N_2- and CO_2-diluted NPFs (a) and PPFs (b). The double flame, triple flame, and blowout regions are also shown.

causing flame liftoff and blowout in NPF [Fig. 11(a)] and PPF [Fig. 11(b)]. Important observations are as follows:

(1) As noted earlier, the undiluted NPF is lifted and stabilized downstream of the burner rim, while the corresponding PPF is stabilized at the burner rim. With the addition of diluent, the liftoff height of NPF first increases gradually, and then quite rapidly until the blowout occurs (cf. Fig. 10). In contrast, the PPF first lifts off from the burner rim due to local extinction caused by dilution, which reduces heat transfer to the rim and the rate of H-atom destruction. Once the flame is lifted, its liftoff height increases much more rapidly compared to that of a NPF. Consequently, its liftoff height exceeds that of a NPF, and the diluent mole fraction required for its extinction (through blowout) is significantly smaller than that for a NPF. For the results presented in Fig. 10, the CO_2 dilutions required for the extinction of PPF and NPF are 16% and 41%, respectively. The corresponding values for N_2 dilution are 25% and 55%, respectively. In addition, a PPF blows out at a lower height compared to a NPF. The superior blowout characteristics of NPFs are due to the higher amount of fuel contained in the fuel jet, which leads to a lower scale dissipation rate for these flames.

(2) The addition of diluent in the fuel jet reduces the chemical activity in the flame base, as indicated by the reduced temperature. As the flame gets weaker, it shifts further downstream to a stabilization location corresponding to a lower scalar dissipation rate (χ), defined as $\chi=2D_{\text{F-}mix}(\nabla f)^2$, where $D_{\text{F-mix}}$ is the fuel diffusivity with respect to the mixture. Figure 12 presents χ plotted versus the axial position along the stoichiometric mixture fraction line for various NPFs and PPFs. For each case, the flame is located at the minimum χ value. The addi-

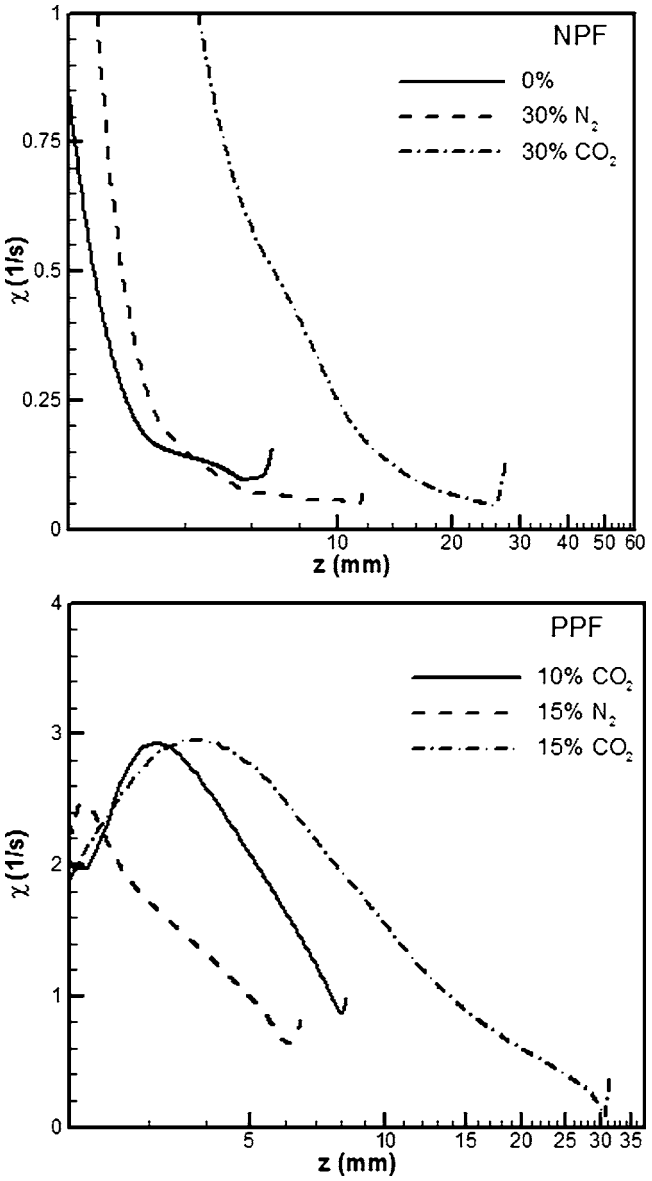

FIG. 12. Scalar dissipation rate (χ) plotted versus the axial position (z) along the stoichiometric mixture fraction line for N_2- and CO_2-diluted NPFs (top) and PPFs (bottom).

tion of diluent increases the local scalar dissipation rate while decreasing the flame reactivity. (The effect of fuel stream dilution on the flame reactivity and scalar dissipation rate is further discussed in the next section.) Consequently, the flame moves downstream to a location of smaller χ in order to achieve a balance between scalar dissipation rate and reaction rate. For a mole fraction of CO_2 greater than 41% (or that of N_2 greater than 55%), the NPF blows out as it cannot find a stabilization point within the computational domain [cf. Fig. 11(a)]. The corresponding mole fractions of CO_2 and N_2 for the blowout of PPFs are 16% and 25%, respectively. The existence of a triple flame structure at the flame base also plays an important role in the stabilization of lifted flames in the far field region. This aspect is discussed in the next section.

(3) For low diluent concentrations, the PPF is located at a lower axial position compared to the NPF. However, as the diluent concentration exceeds a critical value, the PPF shifts to a higher axial location compared to the NPF. Thus, a PPF exhibits a greater sensitivity to fuel stream dilution compared to a NPF (cf. Figs. 10 and 11).

(4) For the same diluent mole fraction, CO_2-diluted flames are lifted higher compared to N_2-diluted flames. Moreover, the diluent mole fraction required for the extinguishment (through blowout) of CO_2-diluted flames is smaller than for N_2-diluted flames, although their liftoff heights at extinction are generally similar for the two cases. As discussed in the next section, this can be attributed to the fact that CO_2 dilution increases the scalar dissipation rate and simultaneously decreases the reaction rate by a larger amount compared to that caused by N_2 dilution.

(5) In the far field region or near the blowout conditions, the liftoff height increases at a faster rate compared to that in the near field. This could be due to the fact that the fuel stream dilution increases the scalar dissipation rate and/or decreases the reaction rate in a nonlinear manner. In addition, both the NPFs and PPFs stabilized in the far field region have a triple flame structure at the base, and a balance between the triple flame speed and local flow velocity also plays a role in the stabilization of these flames. This aspect is further discussed in the next section.

(6) A previous investigation[28] demonstrated that with air stream dilution, methane-air NPFs blow out in a burner-attached mode or in a lifted mode close to the burner. Our simulations indicate that it is possible to establish lifted methane-air NPFs using fuel stream dilution.

Flame stabilization mechanism

Flame liftoff and stabilization are complex processes involving transport, partial premixing, flame propagation, scalar dissipation, and extinction.[33,34] The stabilization of lifted nonpremixed laminar flames has generally been explained based on the existence of a triple flame structure at the base of a lifted flame, and a dynamic balance between the triple flame speed and the local flow velocity.[4–6] This stabilization mechanism is more meaningful for flames that are stabilized in the far field. For flames stabilized in the near field, Takahashi and Katta[8] hypothesized stabilization by the existence of a reaction kernel in which a dynamic balance is maintained between the characteristic reaction rate and scalar dissipation rate. In order to examine these hypotheses in the context of the present simulations, we computed the scalar dissipation rate and flame speed for various N_2- and CO_2-diluted flames.

Figure 12 presents the scalar dissipation rate (χ) versus axial position along the stoichiometric mixture fraction line for several simulated flames. As noted earlier, the flame is stabilized at a location of minimum χ. The effect of fuel stream dilution is to decrease the flame reactivity, as illustrated by the decrease in flame temperature (cf. Fig. 8), and increase the local scalar dissipation rate. The increase in χ is

due to the fact that the fuel stream dilution increases the stoichiometric mixture fraction value (f_s), and thereby shifts the f_s contour from oxidizer region to mixing layer region, which is characterized by large mixture fraction gradients (∇f). Consequently, as the diluent mole fraction is increased, the flame shifts downstream and radially outward to a location of smaller χ in order to achieve a balance between scalar dissipation rate and reaction rate. This stabilization mechanism is consistent with the hypothesis proposed by Takahashi and Katta,[8] and can also be interpreted as a balance between the edge-flame speed (U_F) and the local flow velocity.[43] In fact, the edge flame speed (U_F) has been reported to be a function of the scalar dissipation rate (χ).[14] In addition, the stabilization mechanism can also be used to explain why PPFs are lifted higher than NPF, and CO_2-diluted flames are lifted higher than N_2-diluted flames. As indicated in Fig. 12, the scalar dissipation rate is higher for PPFs compared to that for NPFs. Consequently, PPFs are lifted higher and blow out at a smaller diluent mole fraction compared to PPFs. Similarly, CO_2 dilution decreases flame reactivity, due to the thermal effect, and increases scalar dissipation rate by a larger amount compared to that with N_2 dilution. Consequently, CO_2-diluted flames are lifted higher and blow out at a lower diluent mole fraction compared to N_2-diluted flames.

As discussed earlier, as the flame liftoff height increases, a triple flame structure develops at the flame base (cf. Fig. 7). For these flames, we computed the flame speed (S_L) at the base (triple point) by using the relation[44,45]

$$S_L = -\frac{1}{\rho|\nabla\varphi|}[\nabla\cdot(\rho D\,\nabla\,\varphi)+\omega_\varphi],$$

where the scalar φ is represented by temperature. Figure 13(a) presents the variation of S_L with diluent mole fraction for N_2- and CO_2-diluted NPFs and PPFs. As the diluent mole fraction is increased, the flame speed increases, and the flame is stabilized further downstream in order for S_L to match the local flow velocity. Our results are consistent with those reported by previous researchers. For instance, Kioni *et al.*[10] measured the velocity of a lifted triple flame and found it to be well above the unstreched laminar flame speed of the corresponding stoichiometric premixed fuel-air mixture. In the context of the present study, it should be noted that as the diluent mole fraction is increased, the unstretched laminar flame speed decreases, while the triple flame speed increases, indicating that the ratio of triple flame speed to unstretched laminar flame speed can vary significantly depending upon the mixture and flow conditions. Our results are also in accord with the analysis of Buckmaster,[14] who demonstrated analytically that the flame edge speed (or S_L) increases as the scalar dissipation rate decreases. As noted earlier, with the increase in diluent mole fraction, the scalar dissipation rate (χ) at the flame edge decreases (cf. Fig. 12), and, consequently, the triple flame speed (S_L) increases, as indicated in Fig. 13(a).

The variation of S_L with diluent mole fraction can also be explained from the fact that lifted flames in the present study are positively stretched (at the flame base) and there is a positive correlation between the flame speed and the

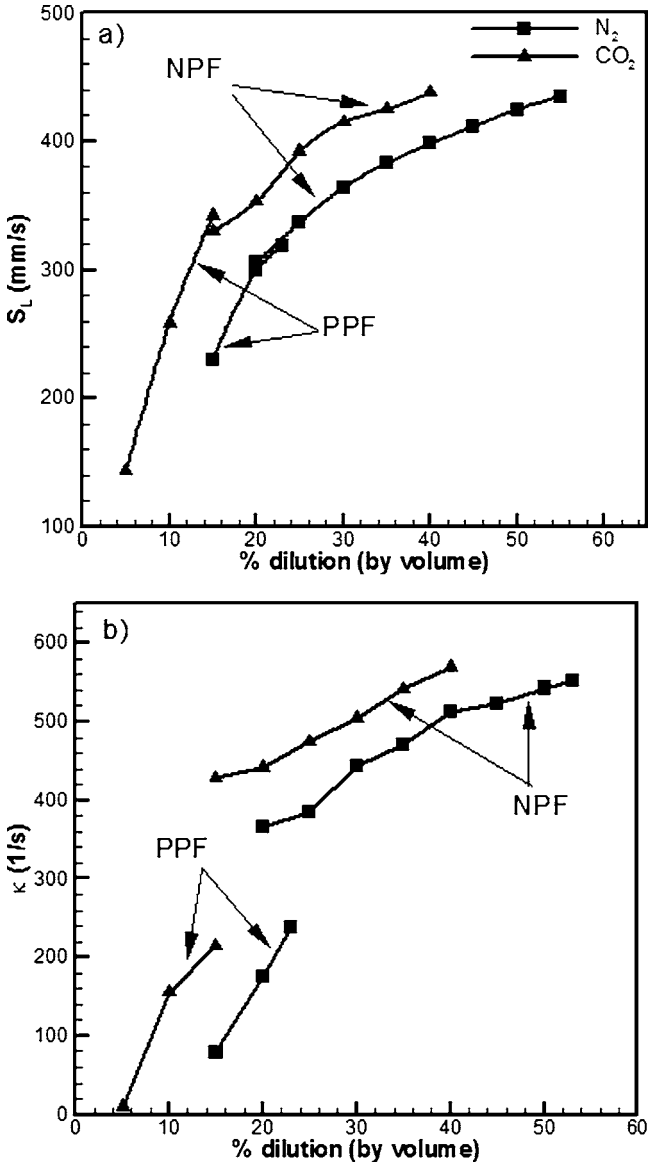

FIG. 13. Stretched laminar flame speed (a) and flame stretch (b) at the flame leading edge (L_{LE}) plotted as a function of diluent mole fraction for the N_2- and CO_2-diluted NPFs and PPFs.

stretch. Figure 13(b) presents the variation of stretch (κ) with the diluent mole fraction for the cases shown in Fig. 13(a). The flame stretch is computed using the relation[44]

$$k = \nabla\cdot \mathrm{V}_{fluid} - \mathrm{nn}{:}\nabla\mathrm{V}_{fluid} + S_\mathrm{L}(\nabla\cdot n).$$

For both the nonpremixed and partially premixed flames, as the flame is lifted higher with the increase in diluent mole fraction, the stretch increases. Moreover, the stretch is higher for CO_2-diluted flames compared to that for N_2-diluted flames, and for NPFs compared to that for PPFs. The correlation between flame speed (S_L) and stretch (κ) is shown in Fig. 14, which presents S_L versus κ for various flames discussed in the context of Fig. 13.

There is a positive correlation between S_L and κ, since these flames are positively stretched and the Lewis number (Le) at the flame base is less than unity. As discussed by Qin *et al.*,[46] the stoichiometric equivalence ratio and the stoichio-

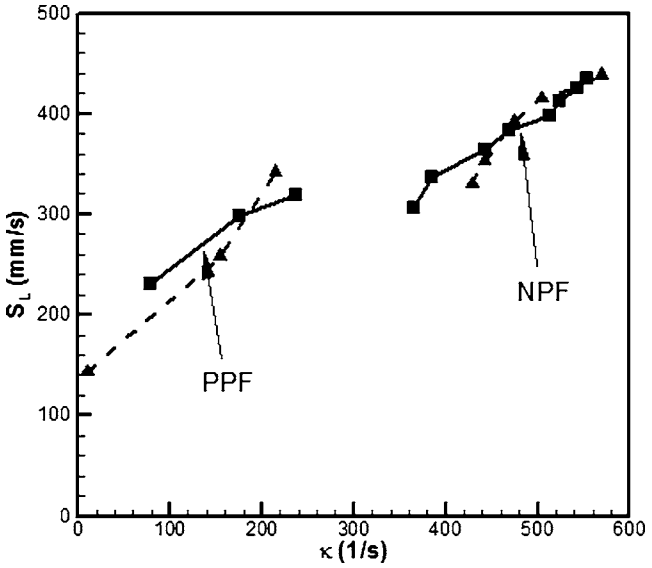

FIG. 14. Stretched laminar flame speed versus flame stretch for various lifted flames discussed in the context of Fig. 13.

metric mixture fraction contours coincide in the cold region, but diverge just ahead of the flame due to product formation. Consequently, the stoichiometric mixture fraction contour leads to a localized lean mixture at the flame base, and for lean CH_4/air mixtures, $Le < 1.0$. Thus, for the positively stretched flame base, its convex nature toward the fresh mixture defocuses the heat, while focusing the deficient species (methane). For $Le < 1.0$, the focusing effect dominates, leading to a positive correlation between flame speed and stretch. Since κ increases with the increase in diluent mole fraction, S_L also increases, as indicated in Fig. 14. In addition, as shown in Fig. 13, κ is higher for CO_2-diluted flames compared to that for N_2-diluted flames, and for NPFs compared to that for PPFs. Consequently, S_L is higher for CO_2-diluted flames compared to that for N_2-diluted flames, and for NPFs compared to that for PPFs.

CONCLUSIONS

We have presented a computational investigation of the flame liftoff, stabilization, and blowout characteristics of nonpremixed (NPF) and partially premixed flames (PPF). Lifted methane-air flames were established in axisymmetric coflowing jets using N_2 and CO_2 as diluents. A time-accurate, implicit algorithm that uses a detailed description of methane-air chemistry and includes an optically thin radiation model was used for simulations. The predictions were validated using measurements of the reaction zone topologies and liftoff heights for both NPF and PPF. Detailed numerical simulations were then used to examine the effects of dilution and partial premixing on the flame liftoff, stabilization, and blowout characteristics, and to analyze previous theories for the stabilization of lifted flames. Important observations are as follows:

(1) The undiluted NPF is lifted and stabilized in a low-velocity region downstream of the burner rim, while the corresponding PPF is stabilized at the burner rim, characterized by significant radical destruction and heat loss to the burner. With the addition of diluent, the liftoff height of NPF first increases gradually, and then quite rapidly until the flame blows out, as it cannot find a stabilization point within the computational domain. In contrast, the PPF first lifts off from the burner rim due to local extinction caused by dilution. Once the flame is lifted, its liftoff height increases much more rapidly compared to that of a NPF. Consequently, its liftoff height exceeds that of a NPF, and the diluent mole fraction required for its extinction (through blowout) is significantly smaller than that for a NPF. In addition, a PPF blows out at a lower height compared to a NPF. The superior blowout characteristics of NPFs are due to the higher amount of fuel contained in the fuel jet, which leads to a lower scalar dissipation rate for these flames.
(2) For flames stabilized in the near field, both NPFs and PPFs exhibit a double flame structure, and their stabilization mechanism involves a balance between reaction rate and scalar dissipation rate, which can also be interpreted as the balance between the edge-flame speed undergoing its local scalar dissipation rate and the local flow velocity. As the diluent concentration is increased, the local scalar dissipation rate increases while the flame reactivity decreases. Consequently, the flame moves downstream along the stoichiometric mixture fraction line to an axial location where it can withstand a lower scalar dissipation rate. Further increase in diluent concentration moves the flame into the far field region, where both NPFs and PPFs exhibit a triple flame structure. Here the flame stabilization also depends on a balance between the triple flame speed and the local flow velocity at the base, and the liftoff height increases more rapidly with increasing diluent concentration. In addition, the flames are positively stretched at the base, and there is a positive correlation between the flame speed and the stretch.
(3) The NPFs and PPFs simulated in the present study exhibit well-organized oscillations induced by buoyant acceleration. As the diluent concentration is increased and the flame is stabilized at a further downstream location, the amplitude of oscillation increases, while the frequency of oscillation remains nearly constant in the range 15–20 Hz.
(4) For the same diluent mole fraction, CO_2-diluted flames are lifted higher compared to N_2-diluted flames. Moreover, the diluent mole fraction required for the extinguishment (through blowout) of CO_2-diluted flames is smaller than that for N_2-diluted flames. This can be attributed to the fact that CO_2 dilution increases the scalar dissipation rate and decreases the reaction rate by a larger amount compared to that caused by N_2 dilution.

ACKNOWLEDGMENTS

This research was supported by the NASA Microgravity Research Division through Grant No. NCC3-688 for which Dr. Uday Hegde and Dr. Kurt Sacksteder serve as the tech-

nical monitors. We thank Andrew Lock for providing the experimental images used for validating the numerical model.

[1] A. J. Lock, A. M. Briones, X. Qin, S. K. Aggarwal, I. K. Puri, and U. Hegde, "Liftoff characteristics of partially premixed flames under normal and microgravity conditions," Combust. Flame **143**, 159 (2005).
[2] H. Phillips, Flame in a buoyant methane layer, Proc. Combust. Inst. **10**, 1277 (1965).
[3] S. H. Chung and B. J. Lee, "On the characteristics of laminar lifted flames in a nonpremixed jet," Combust. Flame **86**, 62 (1991).
[4] B. J. Lee and S. H. Chung, "Stabilization of lifted tribrachial flames in a laminar nonpremixed jet," Combust. Flame **109**, 163 (1997).
[5] G. R. Ruetsch, L. Vervisch, and A. Liñán, "Effects of heat release on triple flames," Phys. Fluids **7**, 1454 (1995).
[6] Y.-C. Chen and R. W. Bilger, "Stabilization mechanisms of lifted laminar flames in axisymmetric jet flows," Combust. Flame **122**, 377 (2000).
[7] F. Takahashi, W. J. Schmoll, and V. R. Katta, "Attachment mechanism of diffusion flames," Proc. Combust. Inst. **27**, 675 (1998).
[8] F. Takahashi and V. R. Katta, "A reaction kernel hypothesis for the stability limit of methane jet diffusion flames," Proc. Combust. Inst. **28**, 2071 (2000).
[9] H. Schlichting, *Boundary Layer Theory*, 2nd ed. (McGraw-Hill, New York, 1979).
[10] P. N. Kioni, B. Rogg, K. N. C. Bray, and A. Liñán, "Flame spread in laminar mixing layers: The triple flame," Combust. Flame **95**, 276 (1993).
[11] T. Plessing, P. Terhoeven, N. Peters, and M. S. Mansour, "An experimental and numerical study of a laminar triple flame," Combust. Flame **115**, 335 (1998).
[12] S. Ghosal and L. Vervisch, "Stability diagram for lift-off and blowout of a round jet laminar diffusion flame," Combust. Flame **123**, 646 (2001).
[13] B. J. Lee, M. S. Cha, and S. H. Chung, "Characteristics of laminar lifted flames in a partially premixed jet," Combust. Sci. Technol. **127**, 55 (1997).
[14] J. Buckmaster, "Edge-flames," J. Eng. Math. **31**, 269 (1997).
[15] UNEP, Montreal Protocol on Substances that Deplete the Ozone Layer, 2004.
[16] N. Vahdat, Y. Zou, and M. Collins, "Fire-extinguishing effectiveness of new binary agents," Fire Saf. J. **38**, 553 (2003).
[17] B. J. Lee, J. S. Kim, and S. H. Chung, "Effect of dilution on the liftoff and non-premixed jet flames," Proc. Combust. Inst. **25**, 1175 (1994).
[18] V. R. Katta, L. P. Goss, and W. M. Roquemore, "Effect of nonunity Lewis number and finite-rate chemistry on the dynamics of a hydrogen-air jet diffusion flame," Combust. Flame **96**, 60 (1994).
[19] Z. Shu, S. K. Aggarwal, V. R. Katta, and I. K. Puri, "A numerical investigation of the flame structure of an unsteady inverse partially premixed flame," Combust. Flame **111**, 276 (1997).
[20] R. Azzoni, S. Ratti, I. K. Puri, and S. K. Aggarwal, "Gravity effects on triple flames: Flame structure and flow instability," Phys. Fluids **11**, 3449 (1999).
[21] R. Siegel and J. R. Howell, *Thermal Radiation Heat Transfer* (Hemisphere Publishing Corporation, New York, 1981).
[22] R. C. Reid, J. M. Prausnitz, and B. E. Poling, *The Properties of Gases and Liquids* (McGraw-Hill, New York, 1987).
[23] N. Peters, *Reduced Kinetic Mechanisms for Applications in Combustion Systems*, Lecture Notes in Physics Vol. m15, edited by N. Peters and B. Rogg (Springer, Berlin, 1993), pp. 3–14.
[24] Z. Shu, C. Choi, S. K. Aggarwal, V. Katta, and I. K. Puri, "Gravity effects on steady two-dimensional partially premixed methane–air flames," Combust. Flame **118**, 91 (1999).
[25] X. Qin, I. K. Puri, S. K. Aggarwal, and V. R. Katta, "Gravity, radiation, and coflow effects on partially premixed flames," Phys. Fluids **16**, 2963 (2004).
[26] H. Xue and S. K. Aggarwal, "Effects of reaction mechanisms on structure and extinction of partially premixed flames," AIAA J. **39**, 637 (2001).
[27] V. R. Katta, L. P. Goss, and W. M. Roquemore, "Numerical investigation of transitional H_2/N_2 jet diffusion flames," AIAA J. **32**, 84 (1994).
[28] V. R. Katta, F. Takahashi, and G. T. Linteris, "Suppression of cup-burner flames using carbon dioxide in microgravity," Combust. Flame **137**, 506 (2004).
[29] F. N. Egolfopoulos and C. K. Law, "An experimental and computational study of the burning rates of ultra-lean to moderately-rich $H_2/O_2/N_2$ laminar flames with pressure variations," Proc. Combust. Inst. **23**, 333 (1990).
[30] V. R. Katta, T. R. Meyer, M. S. Brown, J. R. Gord, and W. M. Roquemore, "Extinction criterion for unsteady, opposing-jet diffusion flames," Combust. Flame **137**, 198 (2004).
[31] Z. Shu, B. Krass, C. Choi, S. K. Aggarwal, V. Katta, and I. K. Puri, "An experimental and numerical investigation of the structure of steady two-dimensional partially premixed methane-air flames," Proc. Combust. Inst. **27**, 625 (1998).
[32] R. Azzoni, S. Ratti, S. K. Aggarwal, and I. K. Puri, "The structure of triple flames stabilized on a slot burner," Combust. Flame **119**, 23 (1999).
[33] N. Peters and F. A. Williams, "Liftoff characteristics of turbulent diffusion jet flames," AIAA J. **21**, 423 (1983).
[34] W. M. Pitts, "Assessment of theories for the behavior and blowout of lifted turbulent jet diffusion flames," Proc. Combust. Inst. **22**, 809 (1988).
[35] R. W. Bilger, "The structure of turbulent nonpremixed flames," Proc. Combust. Inst. **22**, 475 (1988).
[36] M. A. Tanoff, M. D. Smooke, R. J. Osborne, T. M. Brown, and R. W. Pitz, "The sensitive structure of partially premixed methane-air vs. air counterflow flames," Proc. Combust. Inst. **26**, 1121 (1996).
[37] S. Naha and S. K. Aggarwal, "Fuel effects on NO_x emissions in partially premixed flames," Combust. Flame **139**, 90 (2004).
[38] X. Qin, I. K. Puri, and S. K. Aggarwal, "Characteristics of lifted triple flames stabilized in the near field of a partially premixed axisymmetric jet," Proc. Combust. Inst. **29**, 1565 (2002).
[39] A. J. Lock, R. Ganguly, I. K. Puri, S. K. Aggarwal, and U. Hedge, "Gravity effects on partially premixed flames: An experimental-numerical investigation," Proc. Combust. Inst. **30**, 511 (2004).
[40] H. Yamashita, M. Shimada, and T. Takeno, "A numerical study on flame stability at the transition point of jet diffusion flames," Proc. Combust. Inst. **26**, 27 (1996).
[41] H. Guo, F. Liu, and G. J. Smallwood, "A numerical study on NO_x formation in laminar counterflow CH_4/air triple flames," Combust. Flame **143**, 282 (2005).
[42] S. H. Won, S. H. Chung, M. S. Cha, and B. J. Lee, "Lifted flame stabilization in developing and developed regions of coflow jets for highly diluted propane," Proc. Combust. Inst. **28**, 2093 (2000).
[43] S. H. Won, J. Kim, K. J. Hong, M. S. Cha, and S. H. Chung, "Stabilization mechanism of lifted flame edge in the near field of coflow jets for diluted methane," Proc. Combust. Inst. **30**, 339 (2004).
[44] X. Qin, C. W. Choi, A. Mukhopadhyay, I. K. Puri, S. K. Aggarwal, and V. R. Katta, "Triple flame propagation and stabilization in a laminar axisymmetric jet," Combust. Theory Modell. **8**, 293 (2004).
[45] A. Mukhopadyay and I. K. Puri, "An assessment of stretch effects on a flame tip using the thin flame and thick flame formulations," Combust. Flame **133**, 499 (2003).
[46] X. Qin, An investigation of unsteady partially premixed flames, Ph.D. thesis, The University of Illinois at Chicago, 2003.